Solid-State Electronics 230 (2025) 109238

Contents lists available at ScienceDirect

Solid State Electronics

journal homepage: www.elsevier.com/locate/sse

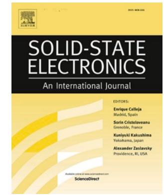

A closed-form model for programming of oxide-based resistive random access memory cells derived from the Stanford model☆

Nadine Dersch [a,b,*], Eduardo Perez [c,d], Christian Wenger [c,d], Mike Schwarz [a], Benjamin Iniguez [b], Alexander Kloes [a]

[a] NanoP, THM University of Applied Sciences, Giessen, Germany
[b] DEEEA, Universitat Rovira i Virgili, Tarragona, Spain
[c] IHP-Leibniz Institute for High Performance Microelectronics, Frankfurt (Oder), Germany
[d] BTU Cottbus-Senftenberg, Cottbus, Germany

ARTICLE INFO

The review of this paper was arranged by Francisco F. Gamiz
Handling Editor: Francisco F. Gamiz

Keywords:
Closed-form
Modeling
Oxide-based
Pulse-programming
Resistive random access memory
Stanford model
Variability

ABSTRACT

This paper presents a closed-form model for pulse-based programming of oxide-based resistive random access memory devices. The Stanford model is used as a basis and solved in a closed-form for the programming cycle. A constant temperature is set for this solution. With the closed-form model, the state of the device after programming or the required programming settings for achieving a specific device conductance can be calculated directly and quickly. The Stanford model requires time-consuming iterative calculations for high accuracy in transient analysis, which is not necessary for the closed-form model. The closed-form model is scalable across different programming pulse widths and voltages.

1. Introduction

Resistive random access memory cells (RRAM) are promising candidates for the development of neuromorphic computing architectures [1–3]. These are non-volatile memories [4,5]. Because of their SET and RESET switching process, they are suitable for reproducing the potentiation and depression of biological synapses [6]. The SET process switches the RRAM into the low-resistive-state (LRS), whereby they are switched on. The RESET changes the status to the high-resistive-state (HRS), in this state the RRAM is switched off [7]. Inside the RRAM there is a filament between the top and bottom electrode. As gap we denote the remaining distance between the filaments grown from bottom and top electrode [8]. In the LRS the gap is minimal, and in the HRS the gap is maximum. RRAMs exhibit device-to-device (D2D) and cycle-to-cycle (C2C) variability [4,9]. The Stanford model (SM) is able to describe the behavior of the RRAM in a circuit simulation. It uses seven different fitting parameters (I_0, g_0, v, V_0, γ_0, β, and α) to represent the varying current–voltage switching curves [7]. In a circuit simulation of a SET or RESET process the equations of the SM are calculated iteratively in a transient analysis, which is time consuming for achieving a high accuracy. Furthermore, in the case of neuromorphic computing, for the purpose of programming a specific conductance value to a synapse, the necessary pattern of the programming voltage has to be determined. In case of an iterative model as the SM this is only possible by further iteration. In this work we present a closed-form analytical model for the SET/RESET process in RRAMs, which allows for a direct and fast calculation of the device current for a given pattern of the programming voltage, without any iterations. The next section describes the RRAM programming scheme considered in this work. Then, the modeling appraoch is described and its limitations are discussed. After the verification of the model, an investigation of its scalability follows.

2. Pulse-programming of resistive random access memories

To change the state of the RRAM from HRS to LRS and LRS to HRS, a train of voltage pulses is used here for programming. These pulses can be

☆ This article is part of a special issue entitled: 'EuroSOI-ULIS 2025' published in Solid State Electronics.

* Corresponding author.
E-mail addresses: nadine.dersch@ei.thm.de (N. Dersch), alexander.kloes@ei.thm.de (A. Kloes).

https://doi.org/10.1016/j.sse.2025.109238

Available online 3 September 2025
0038-1101/© 2025 The Authors. Published by Elsevier Ltd. This is an open access article under the CC BY license (http://creativecommons.org/licenses/by/4.0/).

modified in their amplitude (V_{tb}), their programming pulse width (V_{tb}PW) and their number. The pulse width during the read-out (V_rPW) is the same for every setting and equal to 0.2 V. A representation of these pulses is shown in Fig. 1.

This type of programming was used in [10] for binary HfO_2-based RRAM. The structure of RRAM consists of 150 nm TiN/8nm HfO_2/7nm Ti/ 150 nm TiN. Fig. 2 shows the results for 128 measured RRAM devices for SET (a) and RESET (b) operations. The average value of D2D variations is shown and one measurement is highlighted. This measurement represents a typical switching behavior of the RRAM cell. After 100 pulses, the RRAM is clearly on or off, but it does not switch directly on the first pulse.

3. The closed-form model

With the closed-form model (CFM) presented here, faster calculations are possible than with the SM. The application area is in the programming of RRAMs. For example, a RRAM with a certain conductance value is required for a circuit. The initial parameter gap_{ini}, corresponding to an initial conductance, is known and the RRAM is to be programmed to a specific gap distance (*gap*). The programming is carried out via pulses with constant amplitude V_{tb}. The CFM calculates which total pulse duration is required (or how many voltage pulses of a specific duration) to obtain a specific *gap* (corresponding to a conductance).

The difference between SM and CFM is the calculation of the parameter *gap*. Both models use equation (1) [7] for the current.

$$I = I_0 \bullet \exp\left(\frac{-gap}{g_0}\right) \bullet \sinh\left(\frac{V_{tb}}{V_0}\right) \tag{1}$$

V_{tb} corresponds to the voltage applied from the top to the bottom electrode. The voltage coefficient V_0, the gap coefficient g_0 and the prefactor I_0 refer to experimental data [7]. In the SM the *gap* is calculated iteratively using equations (2)–(4) [7]. Where I_{tb0} is the last current value during the iterative calculation and T is the local temperature at the point where the filament is formed, which varies over time t.

$$\frac{dgap}{dt} = -v_0 \bullet exp\left(\frac{-E_A}{k_b \bullet T}\right) \bullet sinh\left(\gamma \bullet \frac{a_0}{t_{ox}} \bullet \frac{q \bullet V_{tb}}{k_b \bullet T}\right) \tag{2}$$

$$\gamma = \gamma_0 - \beta \bullet gap^{\alpha} \tag{3}$$

$$T = T_{ini} + abs(V_{tb} \bullet I_{tb0} \bullet R_{th}) \tag{4}$$

The field local enhancement factor γ is calculated using the fitting parameters β and α which describe the slope and curvature of the RESET curve. The fitting parameter γ_0 describes the switching point in the SET and v_0 the knee-point voltage of RESET. For more details on model parameters of the SM please refer to [7].

The following simplifications apply to the calculation of the parameter *gap* for the CFM:

1. Temperature $T = \text{const.}$
2. $\sinh(x) = \frac{1}{2}e^x$ for SET ($V_{tb} \gg \frac{k_b \bullet T}{q}$)
3. $\sinh(x) = -\frac{1}{2}e^{-x}$ for RESET ($V_{tb} \ll -\frac{k_b \bullet T}{q}$)

Under these assumptions, the following integrals (equation (5)) can be set up. This results in a closed solution for the total programming time t depending on the initial and targeted value of parameter *gap* (equation (6)). The minus is used for SET and the plus for RESET.

$$\int_{gap_{ini}}^{gap_{target}} \exp(\beta \bullet gap^{\alpha} \bullet C \bullet V_{tb}) dgap = \pm \int_0^t A d\tau \tag{5}$$

$$t = \pm \frac{1}{A}\left(F\left(gap_{target}\right) - F(gap_{ini})\right) \tag{6}$$

$$A = B \bullet \exp(\gamma \bullet C \bullet V_{tb}) \tag{7}$$

$$B = \frac{1}{2} \bullet V_0 \bullet \exp\left(-q \bullet \frac{E_A}{k_b \bullet T}\right) \tag{8}$$

$$C = \frac{a_0}{t_{ox}} \bullet \frac{q}{k_b \bullet T} \tag{9}$$

A function of F(*gap*) can be determined with α = 1, 0.5 or 0.25:

$$F(gap)_{\alpha=1} = \frac{\exp(C \bullet V_{tb} \bullet \beta \bullet gap)}{C \bullet V_{tb} \bullet \beta} \tag{10}$$

$$F(gap)_{\alpha=0.5} = \frac{2 \bullet \exp\left(C \bullet V_{tb} \bullet \beta \bullet gap^{\frac{1}{2}}\right) \bullet \left(C \bullet V_{tb} \bullet \beta \bullet gap^{\frac{1}{2}} - 1\right)}{C^2 \bullet {V_{tb}}^2 \bullet \beta^2} \tag{11}$$

$$F(gap)_{\alpha=0.25} = \frac{4 \bullet \exp\left(C \bullet V_{tb} \bullet \beta \bullet gap^{\frac{1}{4}}\right) \bullet \left(6 \bullet C \bullet V_{tb} \bullet \beta \bullet gap^{\frac{1}{4}} - 3 \bullet C^2 \bullet {V_{tb}}^2 \bullet \beta^2 \bullet gap^{\frac{1}{2}}\right)}{C^4 \bullet {V_{tb}}^4 \bullet \beta^4} + \frac{4 \bullet \exp\left(C \bullet V_{tb} \bullet \beta \bullet gap^{\frac{1}{4}}\right) \bullet \left(C^3 \bullet {V_{tb}}^3 \bullet \beta^3 \bullet gap^{\frac{3}{4}} - 6\right)}{C^4 \bullet {V_{tb}}^4 \bullet \beta^4} \tag{12}$$

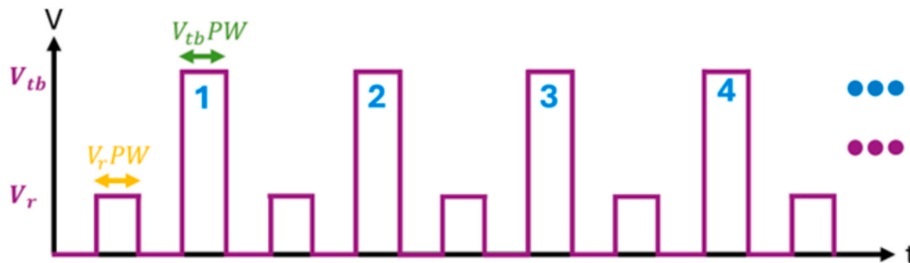

Fig. 1. Visualization of the train of pulses, whose programming voltage (V_{tb}), pulse width for programming (V_{tb}PW) and number of pulses can be adjusted. The pulse width for read-out (V_rPW) is constant for all settings.

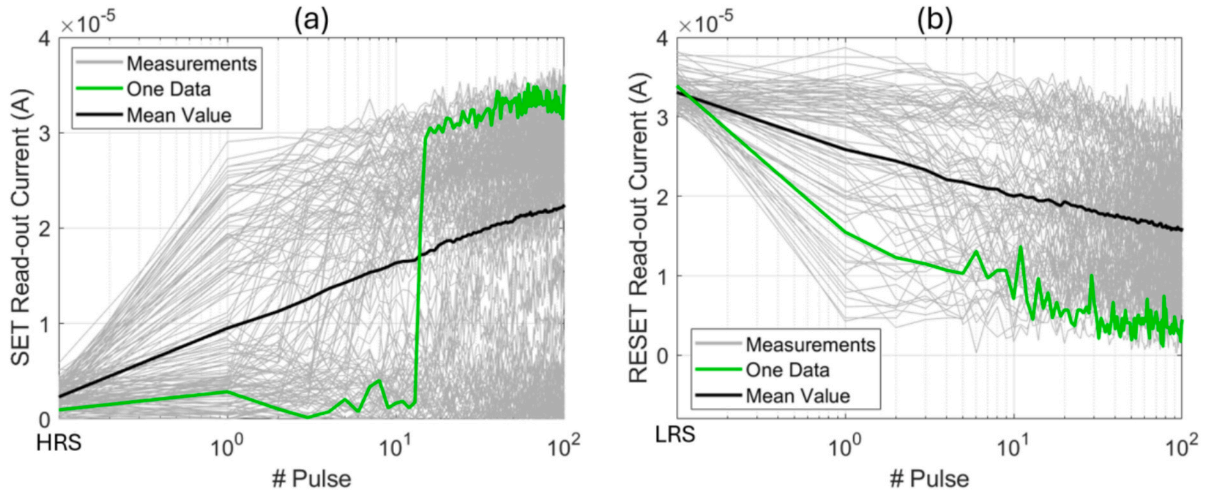

Fig. 2. Representation of 128 measurements (gray), their average value (black) and one marked data (green). In (a) for SET with 100 pulses, $V_{tb} = 0.8$ V and $V_{tb}PW = 1$ µs. In (b) for RESET with 100 pulses, $V_{tb} = -0.8$ V and $V_{tb}PW = 10$ µs. (For interpretation of the references to colour in this figure legend, the reader is referred to the web version of this article.)

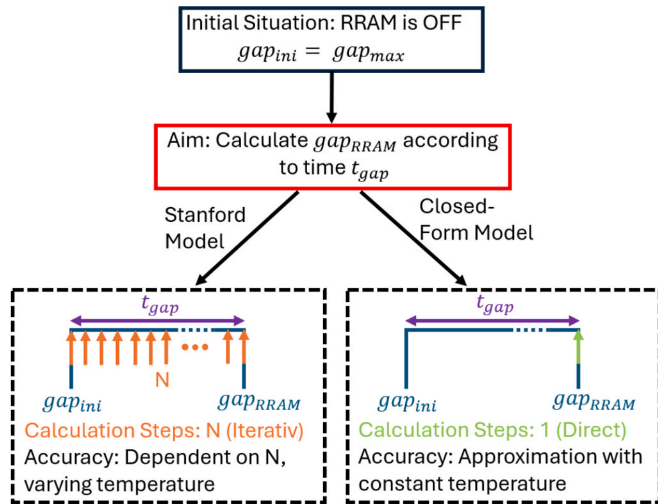

Fig. 3. Illustration of the calculation of the parameter *gap* during the SET process of the RRAM after time *t*. The SM calculates *N* intermediate steps (orange) until the new *gap* is determined. The temperature is adjusted at every step. The larger *N*, the more accurate the result. The CFM calculates the new gap directly (green) without intermediate steps and the temperature is constant. (For interpretation of the references to colour in this figure legend, the reader is referred to the web version of this article.)

The application of the CFM and its advantage over the calculation of the SM are shown schematically in Fig. 3. The fact that the CFM can determine the total programming time *t* corresponds to the typical application: a specific conductivity value of the RRAM is required, for which the filament must be brought to a specific gap distance. The programming voltage is specified, and the current state of the gap parameter is known. By the CFM one can calculate how long the programming must be carried out in order to bring the gap distance to the target value and thus to a specific conductance value. With the SM only the desired programming time can be specified. Therefore, a specific target value for the conductance could only be obtained by iteratively adapting the programming time.

4. Verification of the closed-form model

In the CFM, the temperature is constant and so is a new fitting parameter. To prove that the effect of a varying *T* can be compensated by adjusting the other fitting parameters, we use the SM. The CFM, the SM with variable and constant temperature are compared with measurements in which the RRAMs are programmed over 100 pulses [10] (see marked measurement in Fig. 2). The programming pulse width is 1 µs for SET and 10 µs for RESET. The amplitude is 0.8 V for SET and is −0.8 V for RESET. The results are shown in Fig. 4(a) for SET and Fig. 4(b) for RESET. First, the SM with variable temperature calculated by equations (1)–(4) is fitted to a measurement curve for SET and RESET. Then a constant temperature is set for the SM and also fitted to the measurement curve. Finally, the CFM with the equations (1) and (5)–(9) has been adapted to the measurement.

The comparison of the measurement curve with the SM with variable temperature, with the SM with constant temperature and the CFM shows that all curves are very similar and therefore all three models can be used. The temperature is calculated in the SM according to equation (4). It should be noted that this is a simplified calculation and not a physical quantity. The heat capacity is not considered in the calculation. In the simulation shown in Fig. 4(a), the temperature calculated by the SM at the HRS is 318 K and 561 K after the last pulse. A constant temperature of 470 K was used for CFM simulation.

A transient simulation must be carried out with the SM. Here, using the Spectre Simulator from Cadence, the calculation is performed iteratively up to the specified time. Since the CFM does not have to perform iterative calculations and can calculate the total programming time for a targeted gap distance directly, the calculation is by orders of magnitude faster (depending on necessary time stepping in the transient simulation).

5. Limitation of the closed-form model

As described, a closed-form solution of the integral F(*gap*) is possible for $\alpha = 1$, 0.5 and 0.25. Equation (6) is used to calculate the time after which the programming pulse with voltage V_{tb} has programmed the momentary gap_{ini} to *gap* (desired value). In theory, equation (6) can be rearranged and solved for parameter *gap*. Then, the gap distance called *gap* could be calculated based on parameter gap_{ini} and the pulse time *t*. However, the equation can only be rearranged for $\alpha = 1$. For $\alpha = 0.5$ and 0.25, only the time *t* at which *gap* is reached can be calculated by equation (6).

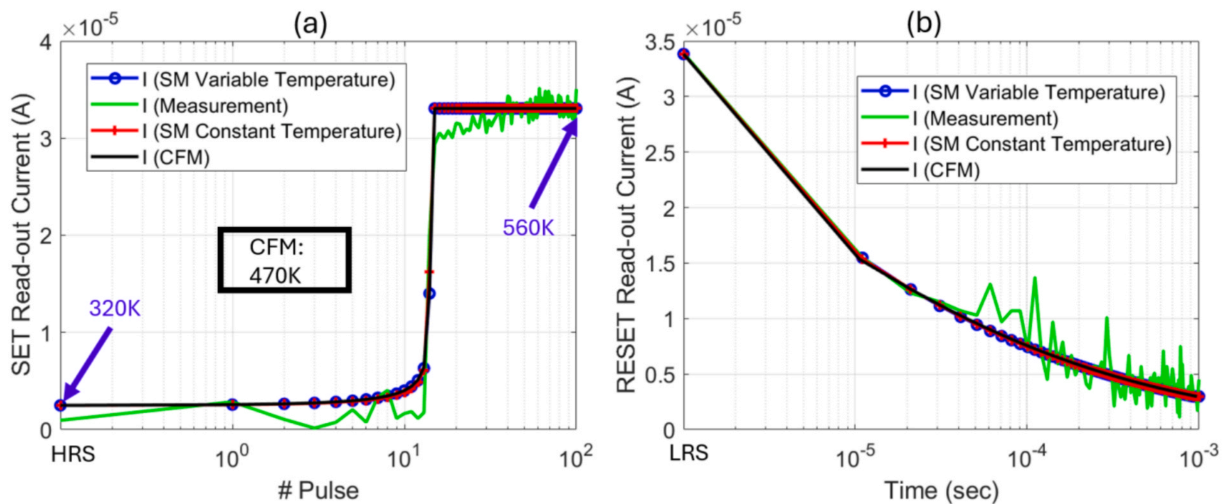

Fig. 4. (a) SET programming with 100 pulses (0.8 V amplitude, 1 μs programming pulse width). (b) RESET programming with 100 pulses (−0.8 V amplitude, 10 μs programming pulse width). Representation of the measurement (green), the SM (blue), the SM with constant temperature (red) and the CFM (black). (For interpretation of the references to colour in this figure legend, the reader is referred to the web version of this article.)

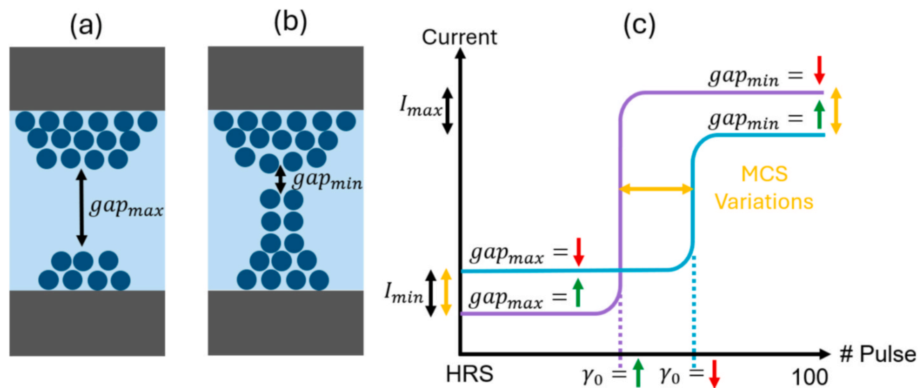

Fig. 5. (a) At $gap_{\max}$ the filament is disrupted. (b) The filament is built up at $gap_{\min}$. (c) The MCS varied $I_{\min}$ with $gap_{\max}$, $I_{\max}$ with $gap_{\min}$ and with γ_0 the switching point. A green arrow indicates that the value has been increased, and a red arrow indicates that it has been decreased. (For interpretation of the references to colour in this figure legend, the reader is referred to the web version of this article.)

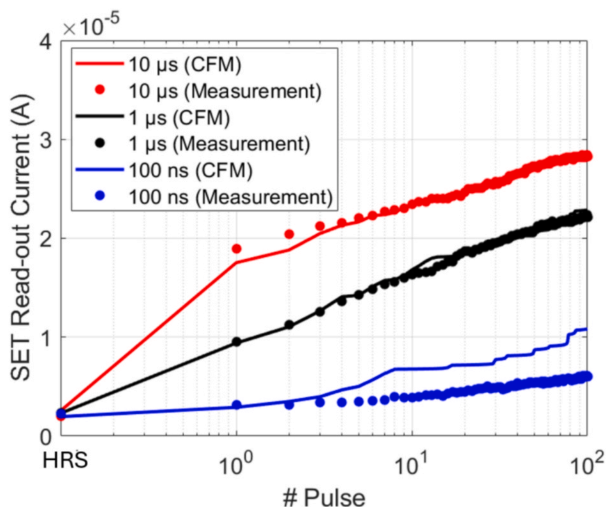

Fig. 6. Average current value of 100 MCS curves at SET with a voltage of 0.8 V and programming pulse widths of 10 μs (red), 1 μs (black) and 100 ns (blue). (For interpretation of the references to colour in this figure legend, the reader is referred to the web version of this article.)

6. Scalability of the closed-form model

Different programming pulse widths (V_{tb}PW) are tested to demonstrate the scalability of the CFM. The measurement data from SET with 0.8 V and programming pulse widths of 10 μs, 1 μs (see Fig. 2) and 100 ns are used [10]. The average value of the current is determined from 128 measured RRAM devices for all three programming modes. A Monte Carlo simulation (MCS) with 100 iterations is then carried out for the CFM, which results in an average current. The parameters $gap_{\min}$, $gap_{\max}$ and γ_0 are varied by the MCS. Fig. 5 shows the influence of these parameters on the current and the structural definition of parameters $gap_{\min}$ and $gap_{\max}$ in the RRAM (γ_0 is a fitting parameter and it has an influence on the switching point). The parameters $gap_{\min}$ and $gap_{\max}$ describe the validity range of the model. The maximum or minimum current value is reached at these limits for the parameter *gap*. A green arrow indicates how the current changes at higher parameter values, and a red arrow indicates how it changes at lower parameter values. The results of the scalability for the programming pulse width are shown in Fig. 6 for the measurements (dots) and the CFM (line).

The average currents of the measurement and the CFM are in good agreement. All modeling parameters were kept constant for all pulse widths. Scalability with respect to the pulse width is therefore ensured. The deviation at a pulse width of 100 ns may be due to the pulse width being too short to heat up the RRAM in the same way as the higher pulse

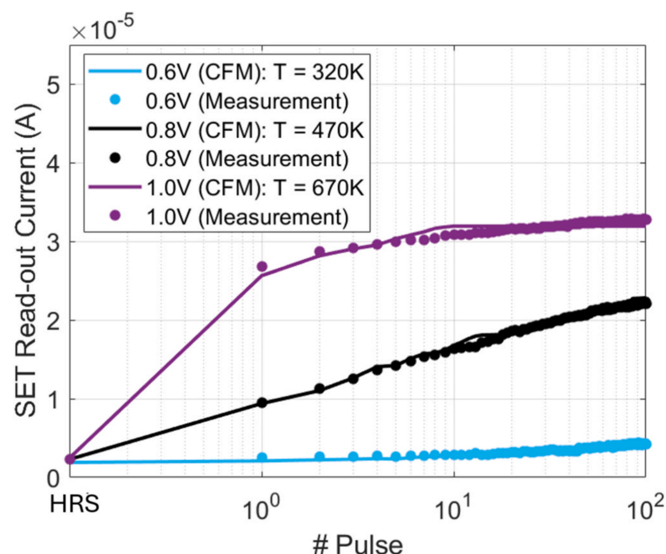

Fig. 7. Average current value of 100 MCS curves at SET with a programming pulse width of 1 μs and voltages 0.6 V (blue), 0.8 V (black) and 1.0 V (purple). (For interpretation of the references to colour in this figure legend, the reader is referred to the web version of this article.)

widths. For a better result, the temperature must be adjusted here. However, because a higher voltage results in a higher power dissipation and therefore a higher temperature in the device, the average temperature used as fitting parameter of the CFM must be adjusted when scaling the voltage. This was tested with the voltages 0.6 V, 0.8 V (see Fig. 2) and 1.0 V with a pulse width of 1 μs [10]. The results are shown in Fig. 7 for the measurements (dots) and the CFM (line). The MCS setting remained the same.

The CFM also shows good agreement with the measurement data for the scalability of the voltage. Here, higher temperatures were required with increasing voltage. It should be noted here that parameter $gap_{\min}$ also had to be adjusted for the case with 1.0 V. All other parameters were also kept constant here. This ensures that the CMF is generally scalable.

7. Conclusions

The comparison of the SM with a variable and a constant temperature shows that both can fit the measurements. Thus, the temperature can be used as a fitting parameter and kept constant, with the effect balanced by other parameters. A closed-form solution for the SM equations has been developed. The CFM simulates a switching cycle in good agreement with the SM and the measurements. The advantage of the CFM is that in contrast to the SM, no time-consuming iterative calculations are necessary. The resulting current can be calculated directly and quickly. In addition, the CFM can be used to determine how long a constant voltage must be applied to obtain a specific current value or conductance. In addition, for the CFM the scalability over different programming pulse widths and voltages has been shown.

CRediT authorship contribution statement

Nadine Dersch: Conceptualization, Data curation, Formal analysis, Investigation, Methodology, Project administration, Validation, Visualization, Writing – original draft. **Eduardo Perez:** Writing – review & editing. **Christian Wenger:** Writing – review & editing. **Mike Schwarz:** Writing – review & editing. **Benjamin Iniguez:** Writing – review & editing, Supervision. **Alexander Kloes:** Writing – review & editing, Supervision.

Declaration of competing interest

The authors declare that they have no known competing financial interests or personal relationships that could have appeared to influence the work reported in this paper.

Acknowledgements

The authors would like to thank the German Research Foundation (DFG) for funding this work under grant 546680029.

Data availability

Data will be made available on request.

References

[1] Huang P, Zhu D, Chen S, Zhou Z, Chen Z, Gao B, et al. Compact model of HfOX-based electronic synaptic devices for neuromorphic computing. IEEE Trans Electron Devices 2017;64(2):614–21. https://doi.org/10.1109/TED.2016.2643162.

[2] Dersch N, Perez-Bosch Quesada E, Perez E, Wenger C, Roemer C, Schwarz M, et al. Efficient circuit simulation of a memristive crossbar array with synaptic weight variability. Solid-State Electron 2023;209:108760. https://doi.org/10.1016/j.sse.2023.108760. ISSN 0038-1101.

[3] Dersch N, Roemer C, Perez E, Wenger C, Schwarz M, Iniguez B, et al., "Fast circuit simulation of memristive crossbar arrays with bimodal stochastic synaptic weights", *2024 IEEE Latin American Electron Devices Conference (LAEDC)*, Guatemala City, Guatemala, 2024, pp. 1-4, doi: 10.1109/LAEDC61552.2024.10555829.

[4] Long S, Lian X, Cagli C, Perniola L, Miranda E, Jiménez D, et al. Compact analytical models for the set and reset switching statistics of RRAM inspired in the cell-based percolation model of gate dielectric breakdown. In: *2013 IEEE International Reliability Physics Symposium (IRPS)*; 2013. 5A.6.1–8.

[5] Zambelli C, Grossi A, Olivo P, Walczyk D, Bertaud T, Tillack B, et al. Statistical analysis of resistive switching characteristics in ReRAM test arrays. In: *2014 International Conference on Microelectronic Test Structures (ICMTS)*; 2014. p. 27–31.

[6] Eryilmaz SB, Joshi S, Neftci E, Wan W, Cauwenberghs G, Wong H-S-P. Neuromorphic architectures with electronic synapses. In: 2016 17th International Symposium on Quality Electronic Design (ISQED); 2016. p. 118–23.

[7] Jiang Z, Wu Y, Yu S, Yang L, Song K, Karim Z, et al. A compact model for metal–oxide resistive random access memory with experiment verification. IEEE Trans Electron Devices 2016;63(5):1884–92. https://doi.org/10.1109/TED.2016.2545412.

[8] Hajri B, Mansour MM, Chehab A, Aziza H, "Oxide-based RRAM models for circuit designers: A comparative analysis," *2017 12th International Conference on Design & Technology of Integrated Systems In Nanoscale Era (DTIS)*, Palma de Mallorca, Spain, 2017, pp. 1-6, doi: 10.1109/DTIS.2017.7930176.

[9] Kloes A, Bischoff C, Leise J, Perez-Bosch Quesada E, Wenger C, Perez E. Stochastic switching of memristors and consideration in circuit simulation. Solid State Electron 2023;201:108606. https://doi.org/10.1016/j.sse.2023.108606.

[10] Perez E, Mahadevaiah MK, Quesada EP-B, Wenger C. In-depth characterization of switching dynamics in amorphous HfO_2 memristive arrays for the implementation of synaptic updating rules. Jpn J Appl Phys 2022;61:1007. https://doi.org/10.35848/1347-4065/ac6a3b.